Supplementary information

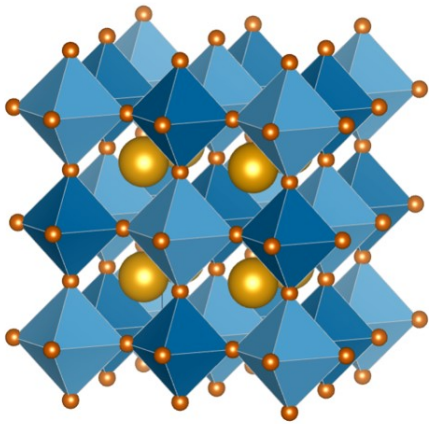

Figure S1. Schematic illustrating double perovskite crystal structure. Yellow balls display A-site cations, red balls display Oxide anions, light and dark blue show octahedrons in which different B-site cations reside (Fe, Mo, Ni). In A-site deficient stoichiometries ($S_{1.8}$FM, $S_{1.8}$FMNi) some A-site vacancies are incorporated.

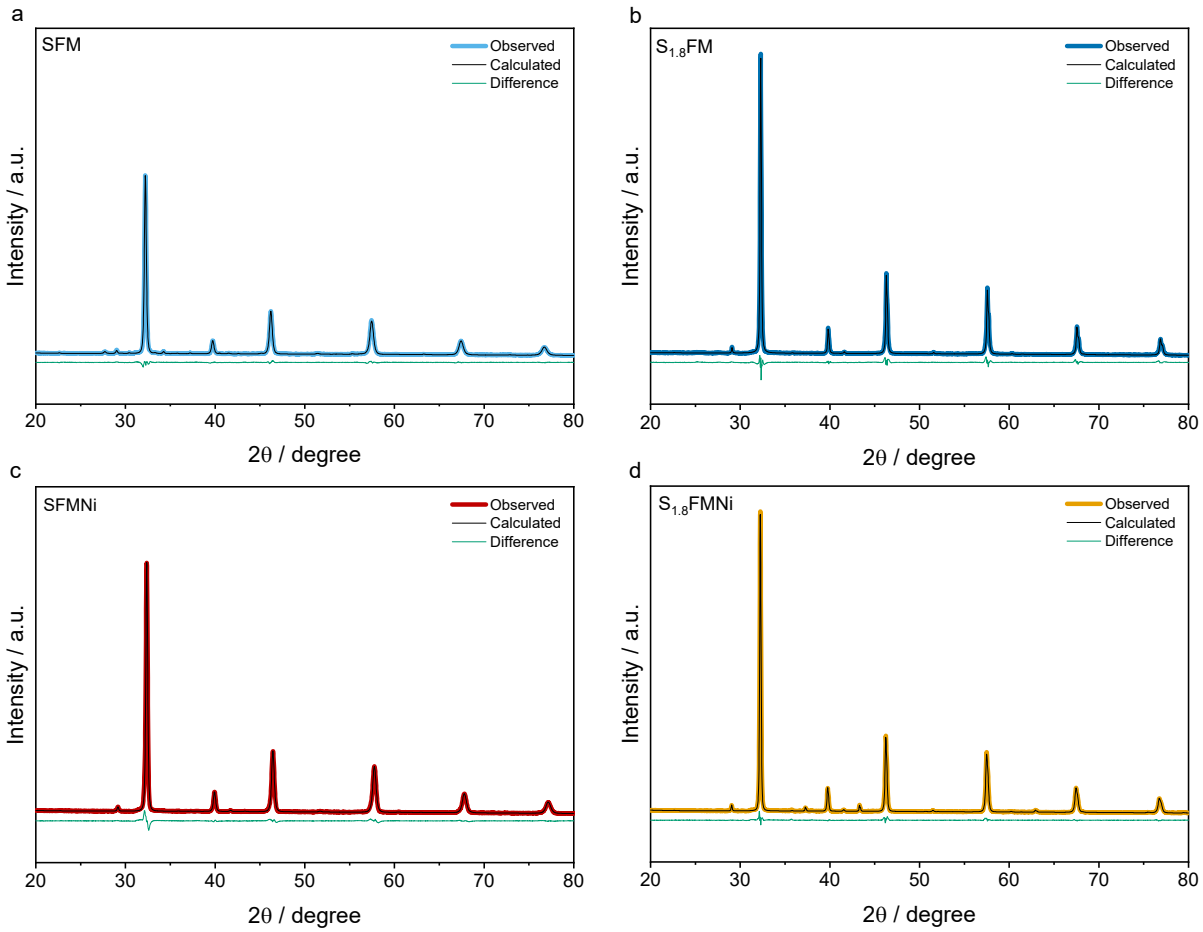

Figure S2. Rietveld refinement of as-prepared materials. **(a)** SFM, **(b)** $S_{1.8}FM$, **(c)** SFMNi and **(d)** $S_{1.8}FMNi$.

Label	Formula	Space group	Goodness-of-fit (χ^2)	Phase purity	Lattice parameter
				wt%	Å
$S_{1.8}FMNi$	$Sr_{1.8}Fe_{1.3}Mo_{0.5}Ni_{0.2}O_{6\pm\delta}$	Cubic, $Fm\bar{3}m$	1.49	96.7	7.850
SFMNi	$Sr_{2.0}Fe_{1.3}Mo_{0.5}Ni_{0.2}O_{6\pm\delta}$	Cubic, $Fm\bar{3}m$	1.50	99.7	7.818
$S_{1.8}FM$	$Sr_{1.8}Fe_{1.5}Mo_{0.5}O_{6\pm\delta}$	Cubic, $Fm\bar{3}m$	1.42	95.5	7.865
SFM	$Sr_{2.0}Fe_{1.5}Mo_{0.5}O_{6\pm\delta}$	Cubic, $Fm\bar{3}m$	1.75	100	7.837

Table S1 Structural parameters of the as-prepared SFM materials obtained from Rietveld refinement fitting

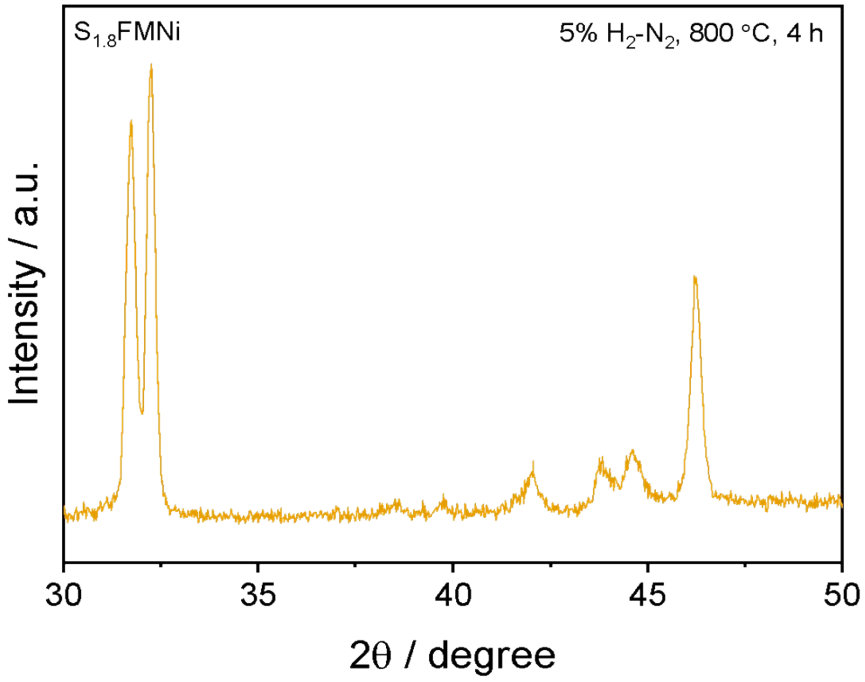

Figure S3. XRD analysis of $S_{1.8}$FMNi after reduction in 5% H_2-N_2 at 800 °C for 4 h, demonstrating phase transition of double perovskite structure into Ruddlesden-Popper phase.

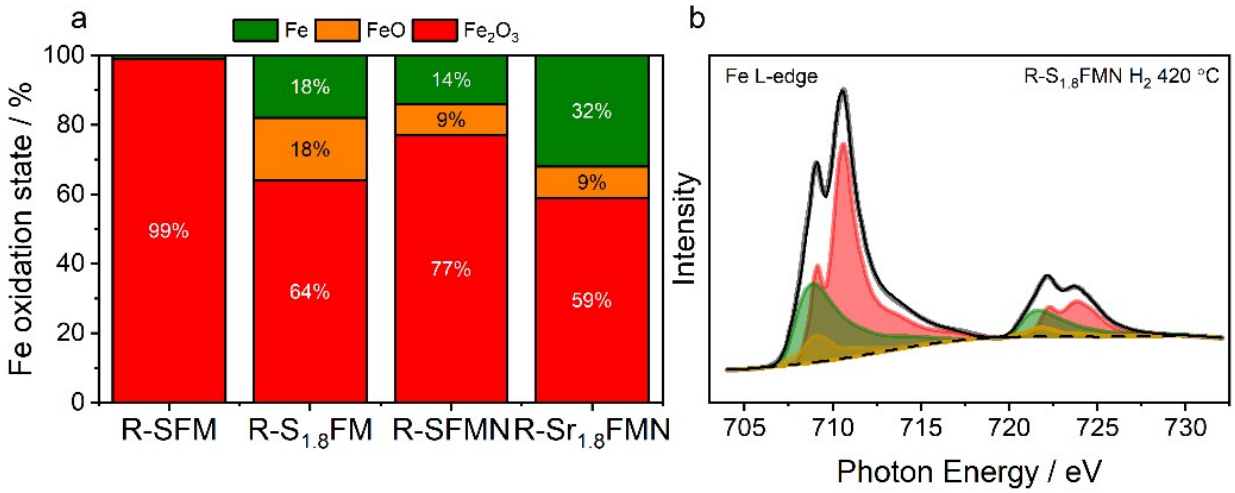

Figure S4. (a) Fe oxidation state distribution (Fe^{3+} vs. Fe^{2+}/Fe^{0}) for SFM-based materials derived from linear combination fitting of Fe L-edge NEXAFS spectra using Fe_2O_3, FeO, and Fe^0 reference spectra. **(b)** Representative Fe L-edge NEXAFS spectrum and corresponding linear combination fit for R-$S_{1.8}$FMNi.

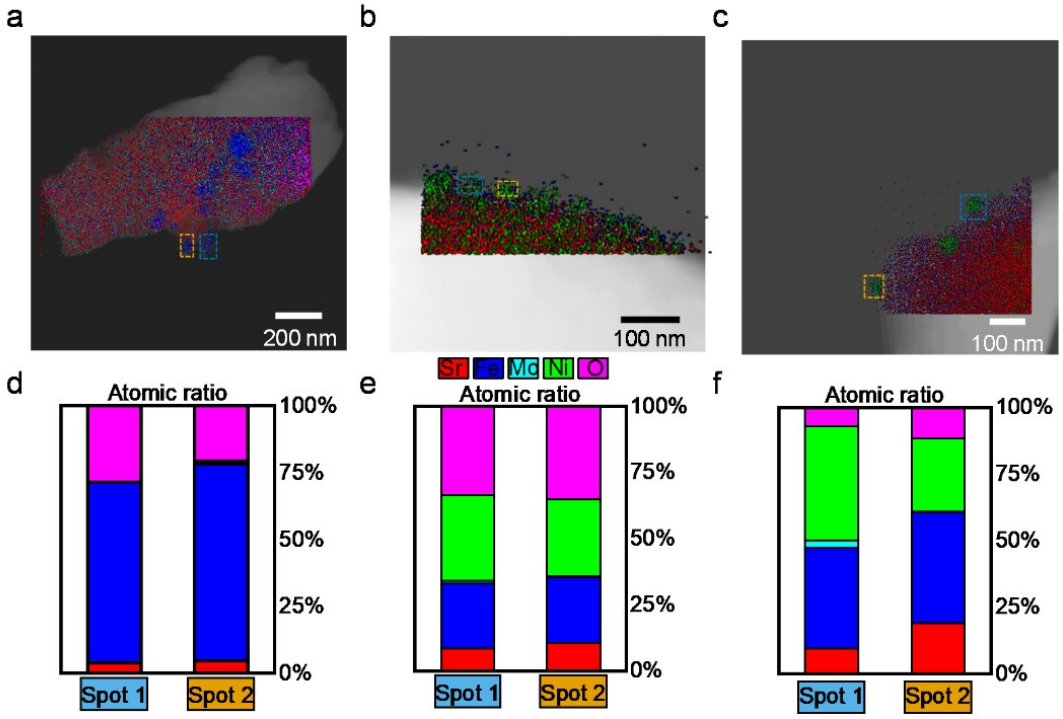

Figure S5. STEM-EDX of reduced powders in 3% H_2O-H_2 at 800 °C for 2 h. a. STEM image elemental mapping on R-$S_{1.8}$FM showing exsolved Fe nanoparticles, b. STEM image elemental mapping on R-SFMNi showing exsolved Fe nanoparticles, c. STEM image elemental mapping on R-$S_{1.8}$FMNi and (d-f) atomic ratio of selected spots showing enrichment of Fe and/or Ni in the exsolved nanoparticles.

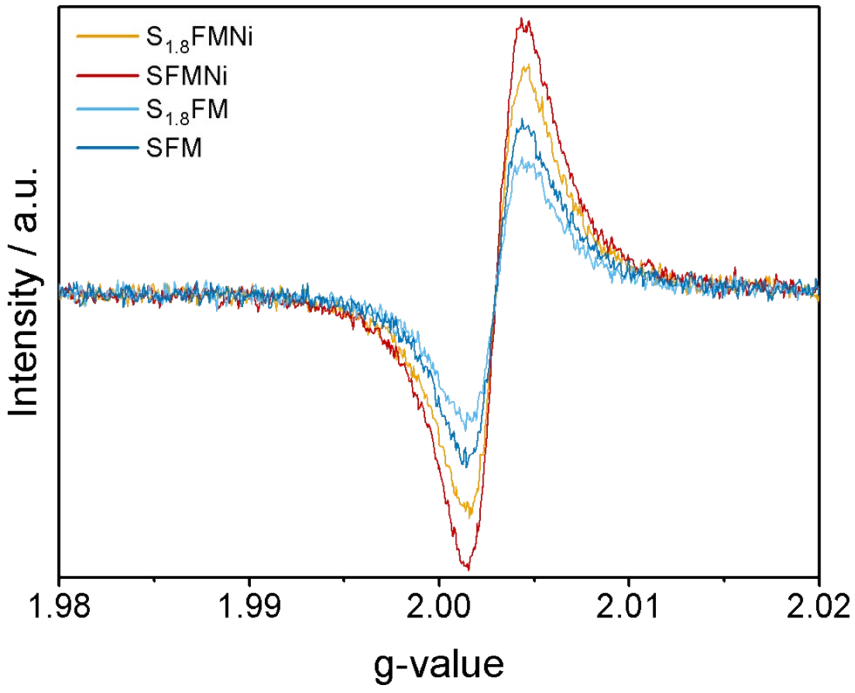

Figure S6. EPR measurements of as-prepared materials

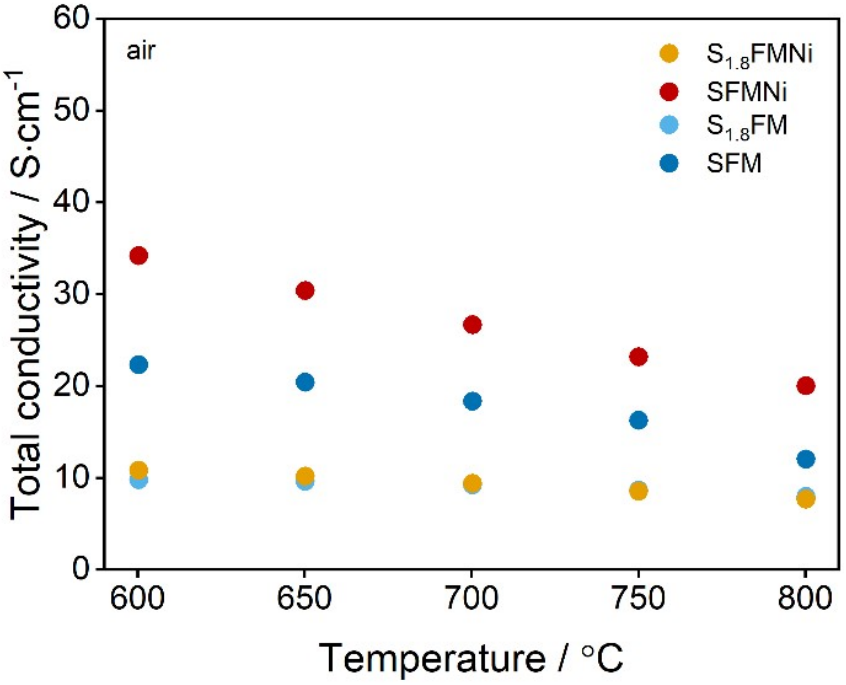

Figure S7. Total conductivity in oxidizing conditions of SFM-based materials shaped in rectangular bars densified at 1300 °C.

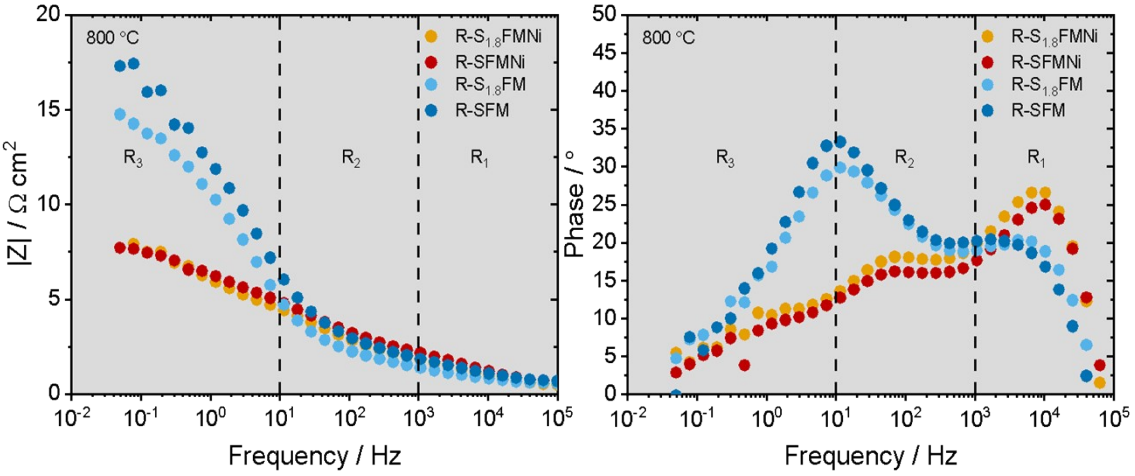

Figure S8. Bode plots of EIS for the co-electrolysis of H_2O and CO_2 at 800 °C under a gas mixture of 25% H_2O, 25% CO_2, and 50% N_2, comparing the effect of different doping strategies on SFM-based electrodes.

a. magnitude of impedance as a function of frequency. **b.** phase angle as a function of frequency. The data highlight the influence of electrode composition on frequency dependent impedance behavior.

Fitting parameters

	Ro	R_1	R_2	R_3	$R_1+R_2+R_3$
	Ω cm^2				
R-SFM	0.71	1.39	2.73	12.88	17.00
R-$S_{1.8}$FM	0.59	0.98	2.62	10.50	14.10
R-SFMNi	0.65	1.73	2.70	2.81	7.23
R-$S_{1.8}$FMNi	0.53	1.25	3.00	3.50	7.75

Table S2 Fitting parameters electrical equivalent circuit for single phase electrodes R-SFM, R-$S_{1.8}$FM, R-SFMNi and R-$S_{1.8}$FMNi in co-electrolysis conditions at 800 °C and 1.3 V as illustrated in the Nyquist plot (**Figure 5b)**.

	Ro	R_1	R_2	R_3	$R_1+R_2+R_3$
	Ω cm^2				
R-SFM	0.77	1.70	5.28	9.88	16.85
R-$S_{1.8}$FM	0.61	1.33	0.63	11.51	13.47
R-SFMNi	0.74	1.27	2.86	3.02	7.14
R-$S_{1.8}$FMNi	0.51	1.54	2.88	2.84	7.25

Table S3. Fitting parameters electrical equivalent circuit for single phase electrodes R-SFM, R-$S_{1.8}$FM, R-SFMNi and R-$S_{1.8}$FMNi in steam electrolysis conditions at 800 °C and 1.3 V during steam electrolysis as illustrated in the Nyquist plot (**Figure 5d)**.

	Ro	R_1	R_2	R_3	$R_1+R_2+R_3$
	Ω cm^2				
R-SFM	0.82	0.69	6.05	12.42	19.16
R-$S_{1.8}$FM	0.89	0.13	0.65	13.89	14.67
R-SFMNi	0.79	0.73	2.61	5.63	8.98
R-$S_{1.8}$FMNi	0.60	0.74	3.96	5.13	9.83

Table S4. Fitting parameters electrical equivalent circuit for single phase electrodes R-SFM, R-$S_{1.8}$FM, R-SFMNi and R-$S_{1.8}$FMNi in CO_2 electrolysis conditions at 800 °C and 1.3 V during steam electrolysis as illustrated in the Nyquist plot (**Figure 5g)**.

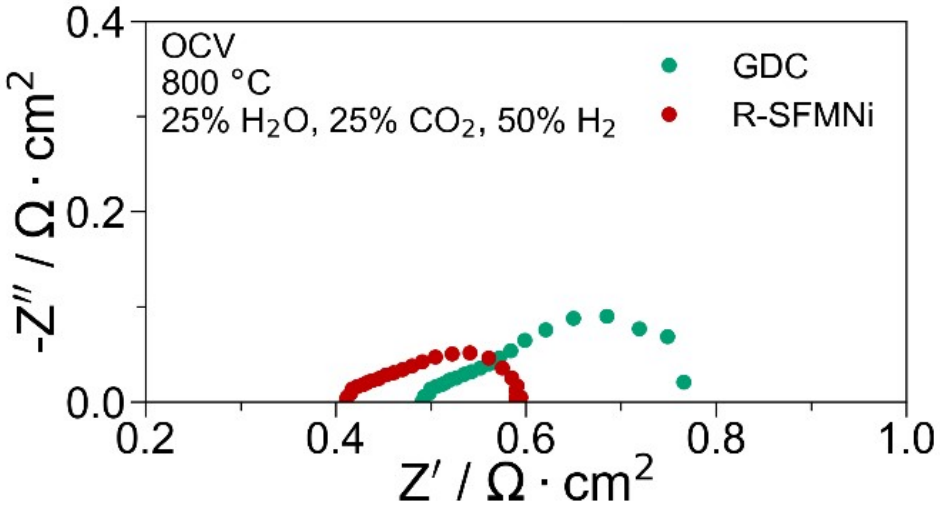

Figure S9. Comparison of resistance contributions for GDC only and R-SFMNi-GDC mixed electrodes at 800 °C in 25% H_2O, 25% CO_2, 50% H_2.

	Ro	R_1	R_2	R_1+R_2
	Ω cm^2			
750 °C	0.53	0.12	0.24	0.36
800 °C	0.41	0.07	0.15	0.21

Table S5. Fitting parameters electrical equivalent circuit optimized cell with R-SFMNi fuel electrode as illustrated in Nyquist plot (**Figure 7a**)

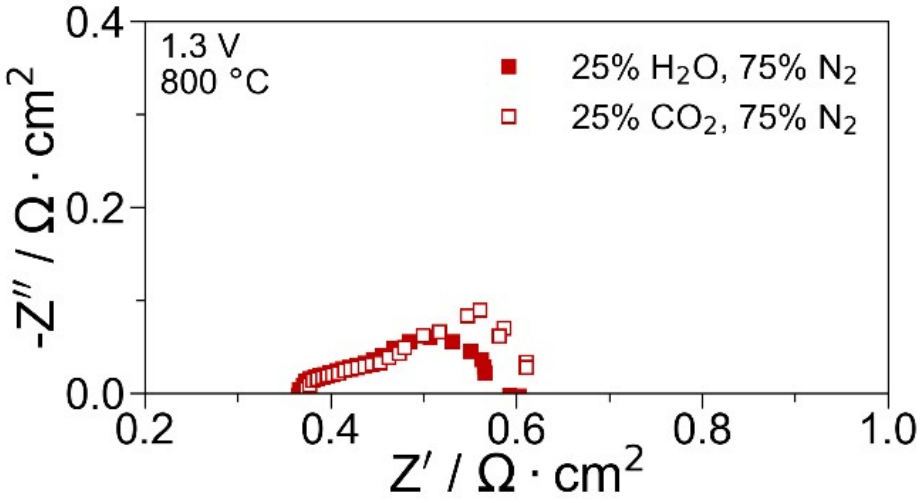

Figure S10. Nyquist plot comparing charge transfer resistance during steam electrolysis and CO_2 electrolysis of a second optimized cell with R-SFMNi fuel electrode.

	Ro	R_1	R_2	R_1+R_2
	Ω cm^2			
25% H_2O – 75% N_2	0.36	0.05	0.18	0.23
25% CO_2 – 75% N_2	0.37	0.06	0.22	0.28

Table S6 Fitting parameters electrical equivalent circuit second optimized cell with R-SFMNi fuel electrode as illustrated in Nyquist plot (**Figure S9**)

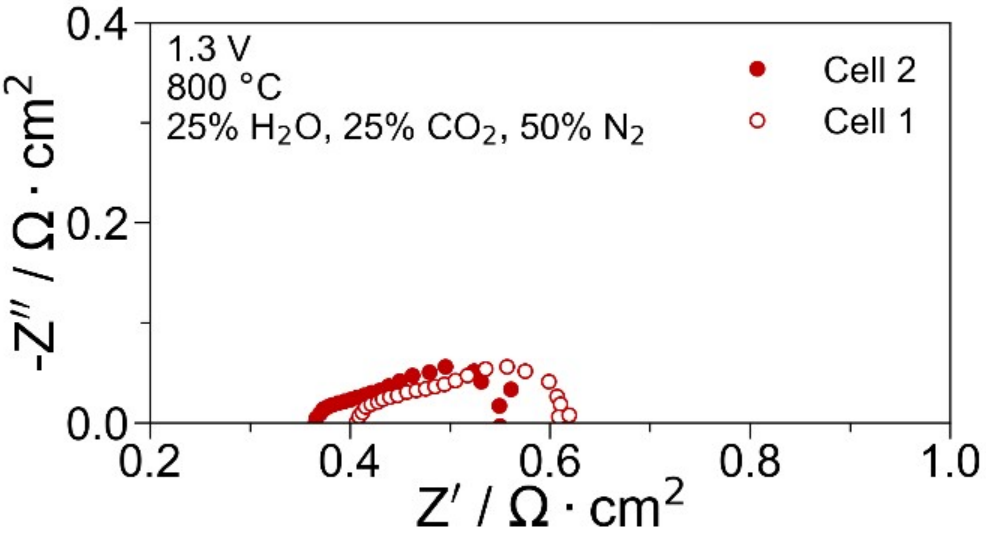

Figure S11. Nyquist plot of a both optimized cells with R-SFMNi fuel electrodes, indicating similar R_p but different R_o values.

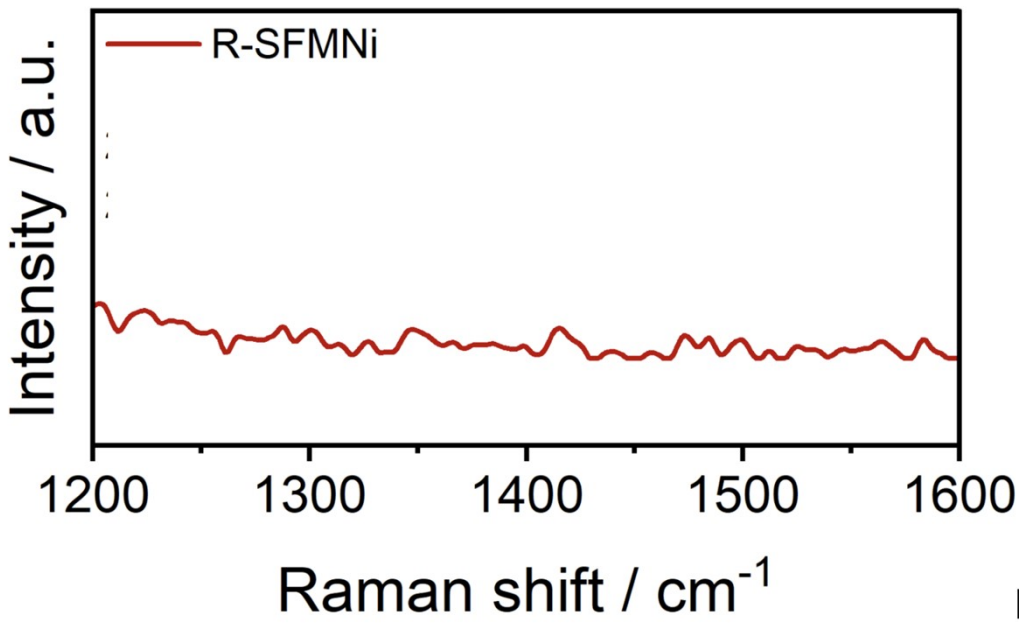

Figure S12. Raman spectra of the SFMNi electrode following stability study which proves the absence of carbon deposition on the spent